An approach for optimization of controllable drilling parameters for motorized bottom hole assembly in a specific formation

Hossein Yavari [a], Mohammad Fazaelizadeh [b], Bernt Sigve Aadnoy [c], Rasool Khosravanian [c], Jafar Qajar [d,e,*], Mostafa Sedaghatzadeh [f], Masoud Riazi [g,h]

[a] *Department of Petroleum Engineering, Amirkabir University of Technology, Tehran, Iran*
[b] *Department of Petroleum Engineering, Faculty of Chemical Engineering, Tarbiat Modares University, Tehran, Iran*
[c] *Department of Energy and Petroleum Engineering, University of Stavanger, Stavanger, Norway*
[d] *Department of Earth Sciences, Utrecht University, Utrecht, the Netherlands*
[e] *Department of Petroleum Engineering, School of Chemical and Petroleum Engineering, Shiraz University, Shiraz, Iran*
[f] *National Iranian Drilling Company, Ahvaz, Iran*
[g] *School of Mining and Geosciences, Nazarbayev University, Astana, Kazakhstan*
[h] *Enhanced Oil Recovery (EOR) Research Centre, IOR/EOR Research Institute, Shiraz University, Shiraz, Iran*

A R T I C L E   I N F O

A B S T R A C T

This study focuses on optimizing drilling parameters when using Positive Displacement Motors (PDMs). In drilling operations involving mud motors, weight-on-bit (WOB) alterations lead to variations in the system's parasitic pressure drop. Consequently, this affects the optimum flow rate and the hydraulic power of the bit. Also, if the flow rate changes, the bit's rotations per minute (RPM) also change. In other words, using PDMs creates a link between the hydraulic system and the drilling speed, such that changing drilling parameters such as the WOB causes changes in the hydraulic system's performance. Therefore, one possible way to optimize the drilling parameters is to consider the drilling rate and hydraulic system simultaneously using a multi-objective approach. This study used an integrated approach encompassing data mining and mathematical modeling, employing a multi-objective framework to identify optimal parameters. The approach was applied to Dariyan Formation drilling data. The data mining approach revealed a well-distributed data set covering optimal and suboptimal zones suitable for optimization. In data mining, the identification of optimal conditions included a WOB of 11500 lb, a rotation speed of 105.8 rev/min, and a flow rate of 843 gpm, leading to an ROP of 44.23 ft/h. In multi-objective optimization, the optimal parameters consisted of a WOB of 14480 lb, a rotation speed of 115 rev/min, and a flow rate of 920.8 gpm, resulting in an ROP of 40.49 ft/h. Comparing optimal results with the drilling data shows a substantial MSE reduction of over 35 %. The results show the good performance of this approach in detecting the optimal and non-optimal drilling variables.

1. Introduction

The need for natural resources is increasing parallel to the quick growth of the global economy [1–4]. The rising need for exploring deeper resources presents challenges [5], and the solution lies in leveraging digitization and optimization techniques to address these issues effectively [6–10]. In conventional drilling, the time spent on drilling constitutes approximately 30 % of the total well completion time. However, in the case of Extended Reach Drilling, this duration can exceed 60 % of the total time required [11]. Furthermore, drilling operations expenses can account for up to 75 % of the overall production

costs [12,13]. Achieving high efficiency, safety, and cost-effectiveness in drilling operations requires optimizing drilling parameters [14]. The goal is to minimize equipment wear and overall drilling costs while achieving the desired rate of penetration [6]. Various methodologies, including statistical analysis, machine learning models, metaheuristic algorithms, and mathematical modeling, can be employed to forecast and ascertain the most optimal collection of parameters, particularly drilling parameters [15–22]. Through the analysis of drilling data and optimization techniques, drilling engineers can identify the most effective drilling parameters for a specific wellbore and formation [12,23].

Typically, drilling parameters are grouped into dynamic and static

variables [14]. Dynamic factors, which can be controllable or uncontrollable, experience changes throughout the drilling process. Controllable parameters include WOB, flow rate, and RPM [14,24,25]. Controllable drilling parameters can be altered fast during a drilling operation [26], making them crucial in drilling optimization. Optimizing controllable drilling variables is the most prominent tactic to boost the drilling rate [14,24,26]. Uncontrollable factors, including drilling fluid density, yield point (YP), and plastic viscosity (PV), pose challenges for drillers as they are difficult and time-consuming to change during drilling operations [14]. On the other hand, static parameters encompass geological characteristics and bit properties, which are predetermined and cannot be adjusted in real-time during regular drilling operations [27]. Fig. 1 depicts the categorization of drilling parameters.

In conventional drilling, controllable drilling parameters are independent, which means that changing one parameter does not change another parameter; for example, when the WOB changes, although it affects the ROP, it does not alter the RPM or flow rate. But when the mud motor is used, the controllable drilling parameters are no longer independent. For example, changing the flow rate causes a change in the RPM. Moreover, an increase in WOB causes an increase in the parasitic pressure drop in the hydraulic system and ultimately causes a difference in the optimal flow rate; in other words, a connection is established between the hydraulic system and other drilling parameters. The primary objective of this study is to mathematically model the impact of the mud motor within the drilling system, examining its influence on the equations governing the Rate of Penetration (ROP), Mechanical Specific Energy (MSE), and the hydraulic system. Subsequently, these established models are utilized to optimize controllable drilling parameters in a particular formation.

Various techniques, including the optimization of ROP, torque on bit (TOB), mechanical specific energy (MSE), vibration, and drilling cost per foot, have been employed to enhance drilling efficiency [28,29]. Some of the most important studies conducted on optimizing drilling parameters are introduced in the following.

In 2016, Moraveji et al. utilized response surface methodology and bat algorithm to estimate and optimize the drilling rate [30]. Chen et al. also presented a new real-time model using MSE to optimize rotary drilling with mud motors in hard formations [31]. In 2019, Hegdeh et al. introduced a novel approach that utilizes machine learning techniques to establish a connection between multiple downhole parameters. By employing the random forests technique and a data-driven modeling approach, individual models were developed for the ROP, MSE, torque on bit (TOB), and stick-slip. The integrated model was then tested on validation data to optimize ROP and MSE. The results demonstrated significant improvements, with an average increase of 31 % in ROP and a 49 % reduction in MSE, showcasing the effectiveness of this optimization model in enhancing drilling performance [32]. In 2019, Liao et al. conducted a study to examine the impact of appropriate feature selection on the estimation and optimization of ROP using intelligent techniques [33].

In 2019, Hegdeh et al. utilized gradient ascent with a random restarts algorithm to determine the optimal control variables, WOB and RPM, for enhancing the drilling speed during drilling. In order to ensure stability, a model for classifying vibrations was utilized as an equality constraint. This constraint served to impose boundaries within the optimization space, preventing the selection of parameters that could potentially result in excessive vibrations. Evaluation of the model using field data demonstrated an average ROP improvement of 14.1 % (10 ft/h) across all formations compared to the measured data [27]. In 2021, Ramba et al. utilized an enhanced play-back methodology to optimize drilling parameters. They also introduced the hydraulic drilling impact (HDI) metric to enhance drilling performance in real-time rotary drilling operations. By monitoring HDI under actual field circumstances, drillers can assess the reliability of the continuing drilling operation [19]. Moazzeni et al. developed the Rain Optimization Algorithm in 2020 as a novel metaheuristic algorithm inspired by rainfall, and they used their approach to optimize drilling operations [34].

In 2020, Alali et al. proposed an innovative hybrid optimization system driven by data, aiming to improve drilling performance by maximizing the ROP while minimizing non-productive time (NPT). This system involves two distinct phases and focuses on adjusting three controllable dynamic drilling variables: RPM, pump flow rate (GPM),
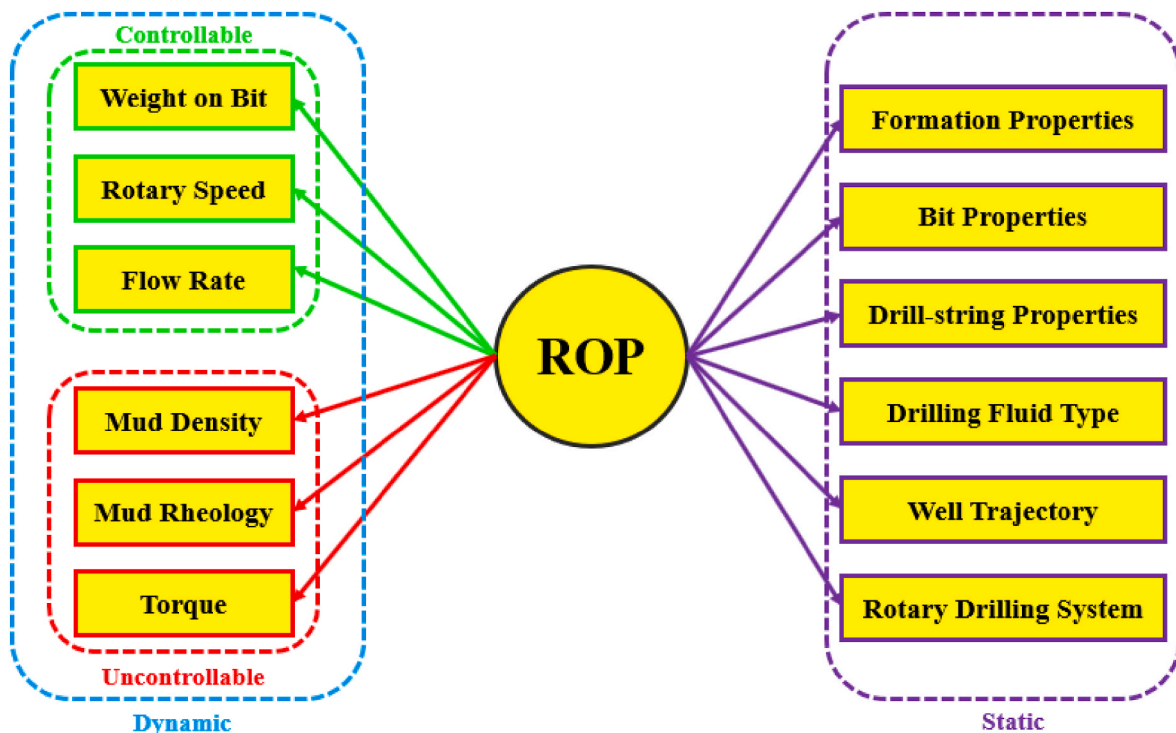

Fig. 1. An illustration of drilling parameters classification concerning ROP optimization [14,24].

and WOB. In Phase One, historical drilling data is utilized to establish a foundation, while Phase Two incorporates real-time adjustments to further enhance drilling efficiency. The primary objectives of this system are to optimize drilling operations and achieve higher ROP while minimizing NPT [14].

In 2021, Wang et al. introduced an optimization and control approach for tool face orientation. Their method incorporates new operating procedures utilizing the surface rocking-pipe-assisted drilling technique. By integrating a drill string dynamics model with various objective functions and manipulated variables, the proposed method identifies optimal control inputs for different slide drilling operations [35]. In 2021, Bani Mustafa et al. improved drilling efficiency through the utilization of response surface methodology to optimize controllable drilling parameters [36]. In 2022, Zang et al. employed logging data from an oil field to develop an intelligent model for predicting the rate of penetration (ROP). The model utilized the random forest algorithm and incorporated a "hard-string" model to compute string drag. To optimize drilling parameters and achieve simultaneous improvements in ROP and drag reduction, the nondominant sorting genetic algorithm-II (NSGA-II) was applied. NSGA-II is a domination-based multi-objective optimization algorithm in a horizontal well [37]. In 2023, Delavar et al. proposed a hybrid machine learning approach that merges multi-objective particle swarm optimization (MOPSO) and random forest (RF) for the optimization of drilling factors. Their objectives were to enhance the amount of ROP and reduce TOB. Geo-mechanical and energy-based features were incorporated into the optimization process. Using a data set from four wells with carbonated reservoirs, the models demonstrated strong correlations between predicted and actual values, with correlation coefficients of 0.97 for TOB and 0.84 for ROP. RF-MOPSO yielded significant improvements, with ROP increasing by 43.8 % and TOB decreasing by 9 % on average across the wells [17].

Previous studies have constraints that make them unsuitable for optimizing drilling parameters for a particular formation when employing a mud motor. Some of the presented methods necessitate substantial data for training their models, as they rely on artificial intelligence (AI) models [12,15,22]. There are only a few drilling data during the drilling of a specific layer, while AI models require a lot of data [22]. Also, many of the presented models do not consider the effect of the mud motor in the well and its relationship with the drilling parameters and hydraulics [36]. In some cases, these studies determine the optimal drilling parameters solely based on maximum drilling speed without considering factors such as drilling hydraulics and mechanical specific energy [28,36,38]. The primary objective of these studies is to enhance drilling performance, with the ROP commonly employed as the principal objective function in such analyses. However, it is imperative to know that attaining a high penetration rate does not necessarily correspond to improved drilling efficiency. It is essential to understand that a high ROP has the potential to give rise to several challenges, which can lead to insufficient removal of cuttings from the wellbore, reduced durability of the drilling bit, and instability difficulties in the wellbore wall [36,39]. Moreover, Burgoyne et al. demonstrated that the highest ROP is not optimal and that the maximum ROP is outside the drilling operation's efficient region [40–42]. For this reason, some studies used other functions such as MSE, vibration, and TOB to optimize drilling parameters [12,27].

The main objective of this study is presenting a data mining procedure and a multi-objective optimization approach to determine optimum controllable drilling parameters for a particular formation being drilled using a positive displacement motor. New hydraulic calculations, ROP, and MSE formulas are derived considering the mud motor. This study stands out from previous research because it can operate effectively with a limited number of data in a specific formation, bypassing the need for extensive data sets for artificial intelligence models [15]. It incorporates a data mining methodology that facilitates the identification of optimal data ranges and the quality of available data. The method is also able to recognize the non-optimal drilling parameters.

Table 1
Details of the bit utilized during the drilling of the 16-inch borehole in well number 3.

Characteristics	Information
Bit type	Insert Bit
IADC Code	435
Nozzle Size	3*20/32
Total Flow Area (TFA)	0.92 in^2
Start Depth	1095
End Depth	1672
Initial Bit Wear	New
Final Bit Wear	2-2-BT-N-F-I-LT-H-R
Bit Wear Coefficient	1.49055*10-7
Bit Friction Coefficient (μ)	0.35

This approach involves an extensive multi-objective modeling process that takes into account ROP, MSE, and drilling hydraulics concurrently, avoiding the singular consideration of a single criterion, such as ROP, for optimal parameters determination. It leveraged a multi-objective genetic algorithm to identify Pareto optimal solutions. Following that, the application of the fuzzy decision-making method facilitated the choice of the most appropriate solution. One notable advantage of this method is its direct reliance on data, eliminating uncertainties. Furthermore, its modeling process is transparent, relying on valid mathematical relationships instead of the artificial intelligence model's black-box nature. This transparency enables thorough verification of each step. This approach can be implemented at various levels, and the precision of the outcomes is closely linked to the quantity and quality of the available data. Finally, the new method and derived formulas were applied to a data set from the Dariyan formation, a limestone formation drilled using a roller cone bit and a mud motor. The results highlight the method's simplicity, accuracy, and efficiency.

2. Data preparation

This study utilizes data from a gas well in the South Pars field. The data was obtained from daily mud logging reports (DMLR), daily drilling reports (DDR), daily geological reports (DGR), and master log reports. Table 1 provides the information about the drill bit used in this section.

In this hole, field data reveal that using a Roller Cone bit produces better outcomes than using polycrystal diamond compact bits. This study focused on the examination of Dariyan formation, which is a limestone layer. Sixty-three drilling data sets were collected during the drilling operations in this particular layer. Table 2 presents comprehensive statistical information regarding the data set.

3. Data mining approach

This procedure is utilized to identify the most suitable parameters by analyzing drilling data within a given geological formation. When using data from multiple wells, it is essential to ensure that uniform drilling bits and tools are employed. Applying this approach separately for each distinct formation within a specific well is recommended. The procedural stages of this method are outlined as follows.

Step	Order
1	**Data Extraction for Each Formation:** Gather data specific to each geological formation encountered during drilling.
2	**Calculation of Mechanical Specific Energy (MSE):** Compute the Mechanical Specific Energy (MSE) and drilling efficiency for the collected data using Eq. (23) and Eq. (24).
3	**Data Sorting Based on Minimum MSE:** Organize the data by sorting it based on the lowest MSE values.
4	**Selection of 10 % to 20 % Data with Lowest MSE:** Choose a subset comprising 10 %–20 % of the data with the minimum MSE.
5	**Selection of 10 % to 20 % Data with Highest MSE:** Choose a subset comprising 10 %–20 % of the data with the maximum MSE.

(*continued*)

Step	Order
6	**Calculation of Average Parameter Values:** Determine the average values of drilling parameters within the selected data set (For all data sets and selected data sets of steps 4 and 5).
7	**Comparison:** Compare the average values of **WOB, RPM,** and **mud weight** calculated in step (6) to determine how increasing or decreasing a parameter impacts ROP and MSE.
8	**Determination of Optimal Flow Rate Window:** Calculate the optimal flow rate window by considering average Weight on Bit (WOB) from step (4) and motor differential pressure (Eq. (10)) according to Maximum Hydraulic Horsepower Eq. (14), and Maximum Jet Impact Force Eq. (15).
9	**Ensuring Flow Rate Alignment with the Optimal Window:** Verify whether the average flow rate of step (4) falls within the established optimal flow rate window and make adjustments if necessary.
10	**RPM Calculation for the Motor:** Calculate the motor's RPM using the determined optimal flow rate using Eq. (30).
11	**Computation of Optimal Surface RPM:** Determine the optimal surface RPM by accounting for the difference between the optimal Bit RPM and motor RPM (Eq. (31)).
12	**Attainment of Optimal Controllable Parameters**

4. Multi objective optimization approach

This part applied a multi-objective optimization strategy using mathematical modeling to determine optimal drilling parameters. Objective functions included hydraulic power, drilling speed, and mechanical-specific energy. The parameters' limitations were selected based on their values in the data set, and the genetic algorithm was employed to find the best solutions. Finally, the fuzzy decision-making method was utilized to identify the best and optimal solutions from the obtained Pareto front. The proposed method for multi-objective optimization of drilling operations is illustrated in Fig. 2. Firstly, the drilling rate model is checked to ensure its consistency with drilling parameters. The new hydraulic system model is coupled with the drilling rate and MSE models. Utilizing hybrid methodologies is the most effective way to develop a comprehensive and versatile optimization strategy [14,32]. Finally, the Pareto optimal solutions of drilling parameters are determined using a genetic algorithm and considering the constraints. Subsequently, the optimal solution is chosen from the available options using the fuzzy decision-making technique.

The subsequent part explains the modeling process for each objective functions, considering the mud motor's inclusion.

4.1. Drilling hydraulic

The hydraulic system of a drilling rig performs several important functions, including removing cuttings, cooling and lubricating the bit, handling formation pressures, stabilizing the well wall, and transferring
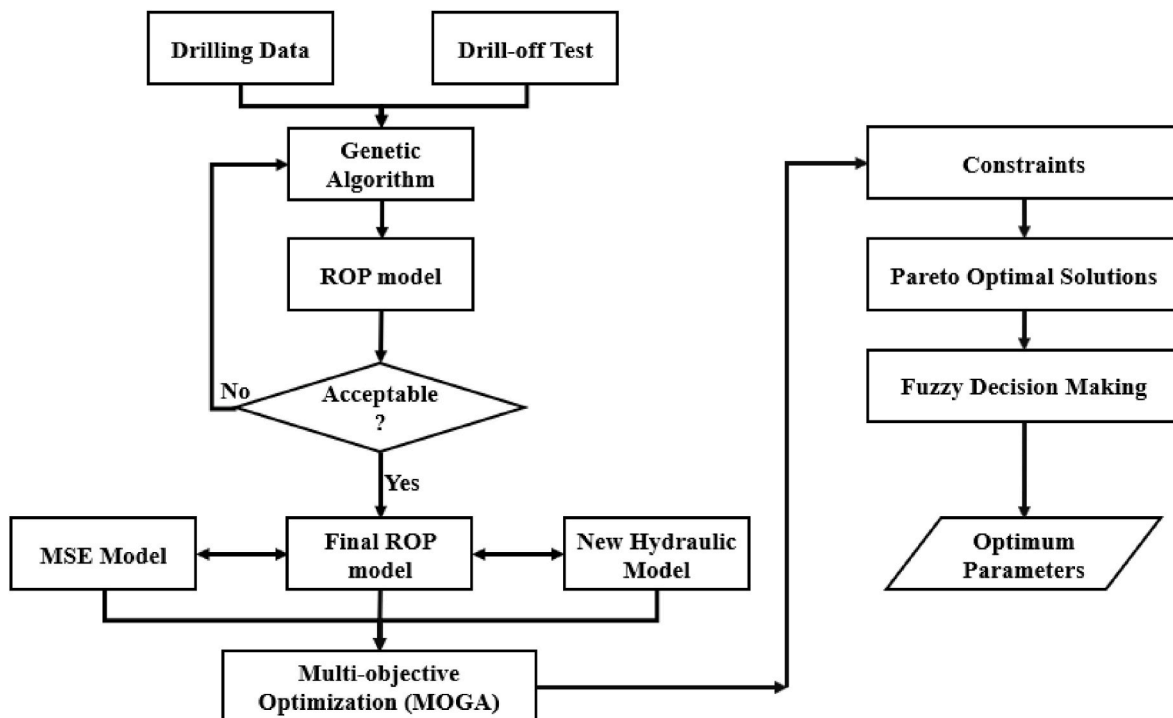
Table 2
Statistical characteristics of drilling data.

No.	Parameter	Unit	Minimum	Maximum	Average	Median
1	TVD	m	1289.29	1347.87	1318.75	1319.32
2	WOB	klb	7	31	20.79	23
3	Bit RPM	rev/min	88	145	123.84	127
4	MW	ppg	9.2	9.2	9.2	9.2
5	Flow Rate	gpm	760	963	872.33	903
6	PV	cp	12	12	12	12
7	YP	$lb_f/100ft^2$	17	17	17	17
8	Motor RPM	rev/min	83	106	95.6	98.9
9	Surface RPM	rev/min	0	40	28.2	40

Fig. 2. Flow chart of multi-objective optimization of drilling parameters.

cuttings to the surface. The productivity of the drilling operation is directly impacted by the hydraulic components involved in the drilling process [43]. The relationship between pump pressure, pressure drop in the bit, pressure drop in the mud motor, and pressure drop in other components is represented in Eq. (1).

$$P_{Pump} = P_{Bit} + P_{Surface} + P_{BHA} + P_{Motor} \qquad (1)$$

where P_{Pump} is the pressure of pump (psi), P_{Bit} is pressure loss in a bit (psi), $P_{Surface}$ contains pressure loss in surface equipment and P_{Motor} is equal to pressure loss in mud motor. The drill string is rotated from the surface by the rotary table, and the rotation speed given to the drill pipe from the surface is called the surface rotation speed ($RPM_{Surface}$). Also, the motor inside the well has a rotation speed that is transferred to the bit by the bearing section, which is called the rotation speed of the motor (RPM_{Motor}). The rotation speed of the bit is equal to the sum of the rotation speed of the motor and the surface rotation speed, which is presented in Eq. (2). Accordingly, there are two types of drilling: sliding (slide drilling) and rotating (land directional market) [35]. When the $RPM_{Surface}$ is zero, and only the motor rotates, it is called sliding drilling, usually used during deviating a well or in deep wells. When the drill string rotates from the surface, it is called rotating [15,35,38].

$$RPM_{Bit} = RPM_{Surface} + RPM_{Motor} \qquad (2)$$

The operational efficacy of a downhole motor is contingent upon the resultant torque it generates and the rotational speed it achieves, both of which are meticulously regulated by the interplay of fluid flow rate and the applied differential pressure. These factors collectively govern the performance and functionality of the downhole motor during drilling operations. In an ideal motor, the rotation speed is determined by the flow rate and the motor's geometry. As fluid flows through the motor, slip flows between the bearings to cool and lubricate the motor components, typically accounting for 5–8 % of the total flow rate. The motor's rotation speed can be calculated using Eq. (3) [38].

$$RPM_{Motor} = \frac{Q - Q_{Slip}}{q_0} \qquad (3)$$

where q_0 is the unit displacement gal/rev, which is equal to the volume of mud required for one rotation of the rotor in the stator, and Q_{Slip} is the slip flow, which is calculated according to the geometry of the motor and its differential pressure from Eq. (4) [38].

$$Q_{Slip} = q_0 * a * exp(b\Delta P) \qquad (4)$$

Here, ΔP is the differential pressure of the motor, and *a and b* are the geometry constants of the motor. Torque is also a motor differential pressure and geometry (lobe configuration) function. The motor output torque is calculated from Eq. (5) [38].

$$T = k * \Delta P \qquad (5)$$

Here, k is a constant number found in the mud motor's performance chart. In other words, there is a linear relationship between the output torque and differential pressure of mud motors. There are two types of pressure loss in the motor. The total pressure loss is calculated from Eq. (6) and Eq. (7) [38].

$$Total\ Pressure\ Drop = No\ Load\ Pressure\ Drop + Differential\ Pressure\ Drop \qquad (6)$$

$$\Delta P_{Total} = \Delta P_{NoLoad} + \Delta P_{Differential} \qquad (7)$$

The WOB influences the differential pressure of the motor as the fluid flows through it. Therefore, the motor should be able to deliver the required torque to rotate the bit. Eq. (8) calculates the torque on the bit [44,45].

$$T = \frac{\mu D_{Bit} WOB}{36} \qquad (8)$$

here, μ is the sliding friction coefficient. It is less than 0.4 for tri-cone bits, with an average value of 0.2 [45]. In 2005, Caicedo et al. presented a correlation for computing the sliding friction coefficient of Polycrystalline Diamond Compact (PDC) bits shown in Eq. (9) [44].

$$\mu = \left(0.9402 e^{\left(-8*10^{-6}*CCS\right)}\right)((-0.8876 \\ * Ln(MW)) + 2.998)(0.0177 * CS + 0.6637) \qquad (9)$$

Here, CCS is the confined compressive strength of the formation in psi, MW is mud weight in ppg, and CS is cutter size in millimeters. The calculation of the differential pressure of the motor is obtained through Eq. (10) by merging Eq. (5) and Eq. (8).

$$\Delta P = \frac{\left(\frac{\mu D_{Bit} WOB}{36}\right)}{k} \qquad (10)$$

As shown in Eq. (10), the pressure drop in the motor depends on the WOB, bit diameter, and type of bit (friction coefficient). It is crucial to ensure that the differential pressure of the motor during drilling remains within its limit [38]. When downhole motors are employed in drilling operations, Eq. (11) is used for the calculation of the pressure drop of a hydraulic system.

$$P_{Pump} = P_{Bit} + P_{Surface} + P_{BHA} + \frac{\left(\frac{\mu D_{Bit} WOB}{36}\right)}{k} + P_{NoLoad} \qquad (11)$$

Using a motor in drilling operations leads to a pressure drop in the hydraulic system, which depends on the WOB. The hydraulic horsepower (HHP) of the bit and jet impact force (JIF) are calculated by Eq. (12) and Eq. (13) [39,46,47].

$$HHP = P_{Bit} * Q \qquad (12)$$

$$JIF = 1.344\sqrt{MW * Q^2 * P_{Bit}} \qquad (13)$$

The pressure loss in the bit is equal to the difference between pump pressure and pressure loss in other areas of the system. The mathematical expressions that represent the hydraulic horsepower and jet impact force are given by Eq. (14) and Eq. (15).

$$HHP = \left(P_{Pump} - \left(P_{Surface} + P_{BHA} + \frac{\left(\frac{\mu D_{Bit} WOB}{36}\right)}{k} + P_{NoLoad}\right)\right) * Q \qquad (14)$$

$$JIF = 1.344\sqrt{MW * Q^2 * \left(P_{Pump} - \left(P_{Surface} + P_{BHA} + \frac{\left(\frac{\mu D_{Bit} WOB}{36}\right)}{k} + P_{NoLoad}\right)\right)} \qquad (15)$$

4.2. Mechanical specific energy

In the process of rotary drilling, two aspects of work are performed: the axial force (WOB) and the rotary component (RPM). Therefore, the total amount of work performed by the drill bit in moving a distance of ΔY can be mathematically defined using Eq. (16) to Eq. (18) [48].

$$Work = Axial\ Work + Rotational\ Work \qquad (16)$$

$$Work = \int_{y_i}^{y_f} F\,dy + \int_{\theta_i}^{\theta_f} \tau\,d\theta = F.\Delta Y + \tau.\Delta\theta = WOB * \Delta Y + T * (\omega_{rad} * \Delta t) \qquad (17)$$

$$Work = WOB * \Delta Y + T * \left(2\pi\omega_{cycle} * \left(\frac{\Delta Y}{ROP} \right) \right) = (WOB * \Delta Y)$$

$$+ \frac{2\pi.RPM.T.\Delta Y}{ROP} \qquad (18)$$

Teale introduced the concept of the MSE in 1964 [48]. MSE indicates the amount of energy consumed to break a certain stone volume and is used as a metric to determine the mechanical efficiency of the work performed on the stone. The MSE is determined by Eq. (19) [44,45].

$$MSE = \frac{Work}{Drilled\ Rock\ Volume} = \frac{Work}{A_{Bit} * \Delta Y} = \left(\frac{WOB}{A_{Bit}} \right) + \left(\frac{2\pi.RPM.T}{A_{Bit} * ROP} \right) \qquad (19)$$

The MSE during drilling is determined by Eq. (20) [44,45].

$$MSE = \left(\frac{WOB}{A_{Bit}} \right) + \left(\frac{2\pi.RPM_{Bit}.T}{A_{Bit} * ROP} \right) \qquad (20)$$

The torque on the bit is one of the needed parameters for calculating the MSE. During drilling, this parameter is measured using measuring systems like MWD. One can also use Eq. (21), published by Pessier in 1992 [45], to compute it. As shown in Fig. 3, he assumed the drill bit was a circular flat rod (shaft), and by specifying a quantity known as the specific coefficient of sliding friction of the bit, which is represented by the letter μ, he was able to calculate the torque on the bit as follows:

The calculation of torque on bit is as follows, in Eq. (21) [45].

$$T = \int_0^{2\pi} \int_0^{\frac{D}{2}} r^2 \mu \frac{WOB}{(\pi/4)D^2} dr.d\theta = \int_0^{\frac{D}{2}} \frac{8\mu WOB}{D^2} r^2 \bullet dr = \frac{8\mu WOB}{D^2} \bullet \frac{D^3}{8*3}$$

$$= \frac{\mu D WOB}{3} \qquad (21)$$

The above equation becomes Eq. (22) in field units [45].

$$T = \frac{\mu D_{Bit} WOB}{36} \qquad (22)$$

The MSE for this hole, taking into account the characteristics of both the drill bit and the motor being utilized, can be calculated using Eq. (23) [32,49].

$$MSE = \left(\frac{WOB}{A_{Bit}} \right) + \left(\frac{120\pi}{A_{Bit} * ROP} \right) \left(RPM_{Surface} + \left(\frac{Q - Q_{Slip}}{q_0} \right) \right) \left(\frac{\mu D_{Bit} WOB}{36} \right) \qquad (23)$$

Teale showed that the lowest achievable Mechanical Specific Energy (MSE) during drilling is equal to the tri-axial compressive strength of the rock (CCS). When the MSE equals the triaxial strength of the rock, drilling efficiency reaches 100 %. In other words, the rock's compressive strength represents the specific energy needed to fracture the rock. At the same time, MSE reflects the work done and energy expended in breaking the rock during drilling. The ratio of these values serves as an indicator of drilling efficiency. Drilling efficiency is calculated from Eq. (24) [17,45,50].

$$Drilling\ efficency = \left(\frac{CCS}{MSE} \right) * 100 \qquad (24)$$

4.3. Rate of penetration

In 1987, Warren developed a drilling model that accounts for the impact of WOB, RPM, Confined Compressive Strength (CCS), and bit diameter on the drilling rate [51,52]. Warren's model underwent modifications by Winters et al., in 1987 and Harland and Hobrock in 1993. The modified Warren model (Eq. (25)) was used to estimate the drilling rate in this article [52–54].

$$ROP = K * W_f \left[\left(\frac{a * CCS^2 D_{bit}^3}{RPM_{Bit}.WOB^2} + \frac{b}{RPM_{Bit}.D_{bit}} \right) + \frac{cD_{bit}\gamma_f PV}{F_{jm}} \right]^{-1} \qquad (25)$$

where F_{jm} is modified jet impact force (klb), γ_f is the specific gravity of mud weight, PV is viscosity (cP), $a, b,$ and c are constants of the model, WOB is weight on bit (klb), RPM is revolution per minute (rpm), CCS is the tri-axial compressive strength of formation (psi), W_f is bit wear function [52]. In this model, F_{jm} is calculated using Eq. (26) and Eq. (27) [39].

$$F_{jm} = \left(1 - \left(\frac{0.15D_{bit}^2}{3D_n^2} \right)^{-0.122} \right) * 0.000516.MW.Qv_n \qquad (26)$$

$$v_n = 0.32 \left(\frac{Q}{TFA} \right) \qquad (27)$$

where D_{bit} is the bit diameter (in), MW is the fluid density (ppg), Q is the mud flow rate (GPM), and v_n is the speed of fluid exiting the drill nozzle in feet per second [52].

The Genetic Algorithm (GA) facilitates the optimization, coefficient identification in mathematical models and the training of Artificial Intelligence models based on experimental data [55–62]. The GA, a meta-heuristic algorithm, was initially proposed by John Holland in the 1960s. It utilizes metaheuristic techniques that simulate the processes of natural selection and genetic mechanisms to explore feasible solution spaces [63–66]. By leveraging the provided drilling data, a GA assists in determining the optimal coefficients for the modified Warren model. The modified Warren model was utilized in this study to optimize the drilling rate, which is briefly shown in Eq. (33).
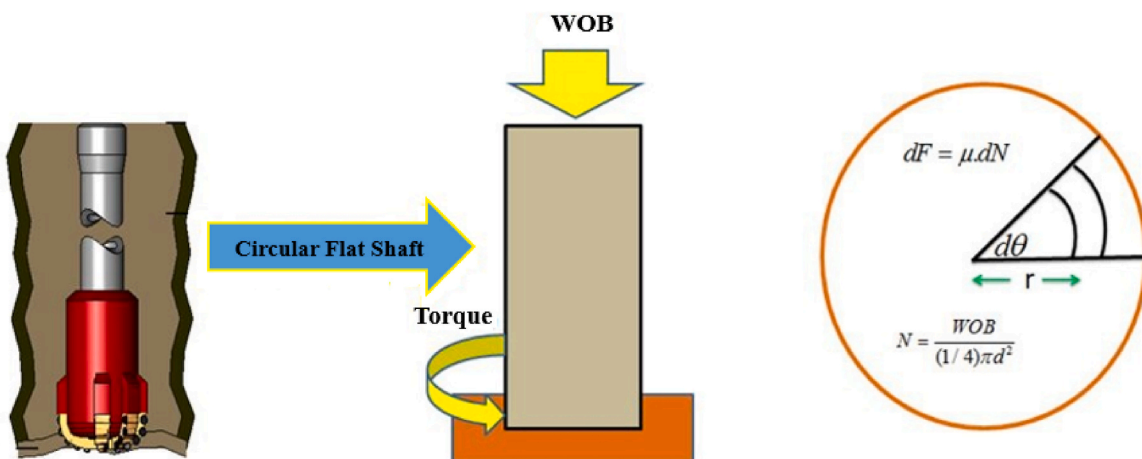

Fig. 3. The simplified representation of the drill bit profile [45].

5. Results and discussion

In the subsequent sections, we present the culmination of our study focused on optimizing controllable drilling parameters within the Dariyan formation. Our investigation hinged on using 63 gathered drilling data points, subject to a data mining approach and a multi-objective mathematical modeling framework. The ensuing results underscore the robust applicability of both methodologies in addressing the intricate challenges associated with drilling operations in this specific geological formation. Through a rigorous examination of the data, we unearthed valuable insights that validate the efficacy of these approaches and offer a promising procedure for enhancing drilling efficiency and decision-making processes within the Dariyan formation.

5.1. Data mining approach

The analysis of drilling data is a crucial preliminary step that should be done before engaging in mathematical modeling or modeling with artificial intelligence. This is essential to ensure the resulting model's accuracy and effectiveness. The presence of a well-distributed pattern in the data and a small amount falling inside the optimal range are crucial factors to consider. When confronted with a situation where the supplied data is suboptimal and lacks a logical relationship, it becomes impractical to train a model successfully and ascertain ideal points through computations. Fig. 4 illustrates the data distribution throughout the Dariyan formation. The controllable parameters have an excellent distribution.

Fig. 5 illustrates the box plot for controllable drilling parameters, ROP, and MSE. Analyzing Figs. 4 and 5 shows that the WOB parameter

falls within the range of 7000–31000 lb, the rotation speed ranges from 88 to 145 rev/min, and the flow rate spans from 760 to 963 *gpm*. These drilling parameters result in speeds ranging between 16.4 and 63.5 ft/h and MSE values ranging from 4879 to 49678 psi. All these parameters exhibit well-distributed values, with no notable concentration around specific values and minimal density variations across data points. Consequently, some of the applied parameters operate efficiently, characterized by a high ROP and low MSE, while others operate suboptimally in the drilling process. Careful data examination readily identifies the parameters within the high-efficiency range.

Another method for assessing the data distribution and quality involves calculating drilling operation efficiency. The efficiency of drilling operation in Dariyan layer was determined using Eq. (28) [17,45]. Fig. 6 illustrates the relationship between drilling efficiency and ROP, followed by a box diagram of drilling efficiency.

$$Drilling\ efficiency = \frac{CCS}{MSE} * 100 = \frac{4000}{MSE} * 100 \qquad (28)$$

in the Dariyan Formation, drilling efficiency ranges from 8 % to 81.9 %, with a mean value of 26.54 %. The box plot illustrates that 75 % of the data falls below 30 % efficiency. This diagram suggests that drilling efficiency effectively outlines data distribution and quality. Some data points are within the optimal region, while others reside in the non-optimal area. Through careful data analysis, one can identify the optimal locations and subsequently include them in the optimization procedure.

In this study, a fixed value of 4000 psi was used to represent the CCS of the Dariyan formation. It is evident that achieving a high level of
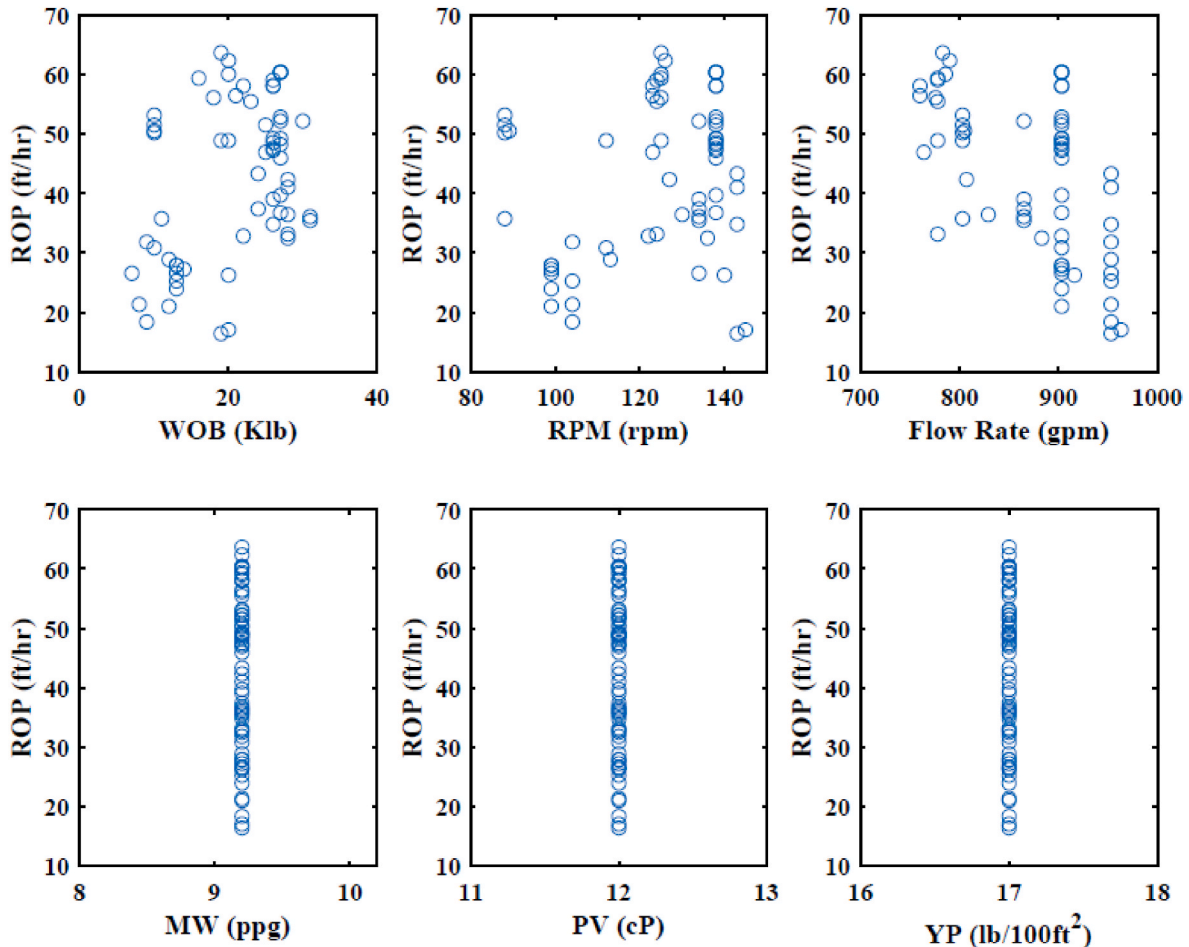

Fig. 4. The schematic representation of data distribution in the Dariyan formation.
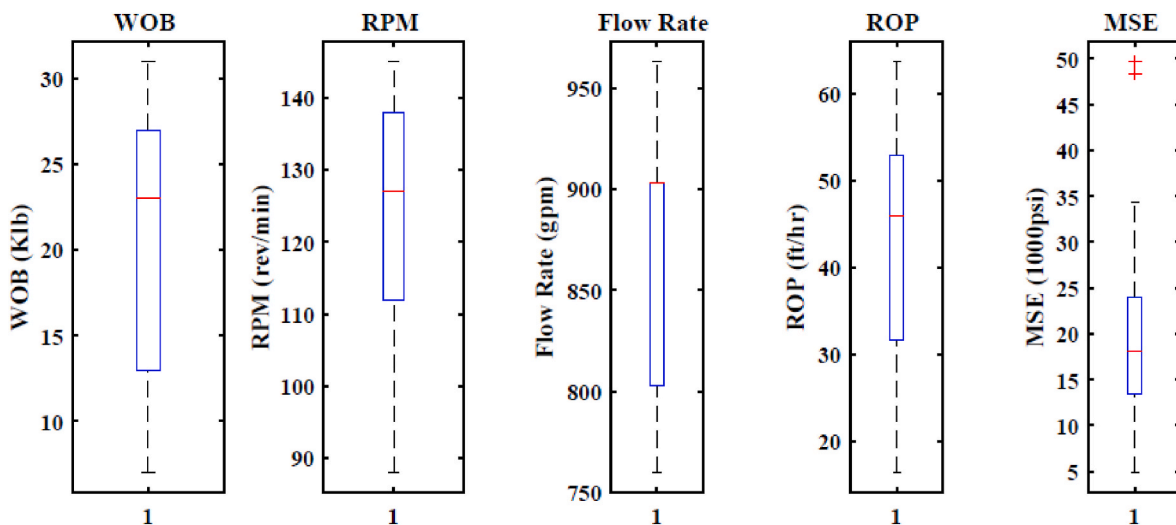
Fig. 5. Box diagram of the controllable drilling variables, ROP, and MSE in the Dariyan layer.
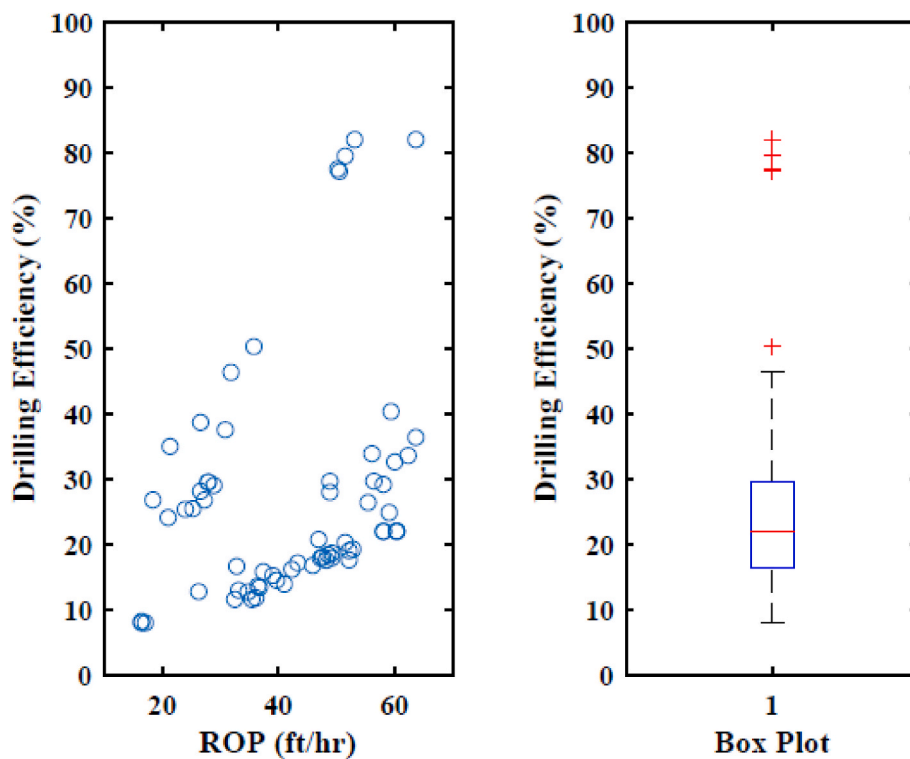

Fig. 6. Distribution and box plot of drilling efficiency in the Dariyan layer.

precision in determining the formation's geo-mechanical parameters significantly enhances the accuracy of the optimization process. For instance, the CCS of the formation plays a crucial role in both efficiency calculations and modeling ROP, thereby improving the overall accuracy of the computations. Figs. 4–6 demonstrate that the data exhibits a satisfactory distribution and quality, making it suitable for the optimization procedure.

The data mining approach was employed to examine the drilling data related to the Dariyan formation. Table 3 displays the 20 % of drilling data set with the least MSE, along with their corresponding average values. These data led to the determination that, within this formation, the optimal values are a WOB of 11.5 *Klb* and an RPM of 105.8 *rev/min*. As can be seen, with the increase in WOB and RPM, the MSE has increased while the ROP has decreased slightly. This shows that

increasing the drilling parameters increases the ROP. In some cases, the ROP may increase a little, but the MSE increases significantly, and this causes the drilling operation to be non-optimized.

Subsequently, with the optimal WOB set at 11.5, the differential pressure of the mud motor was computed. By adding this to the pressure drop of the hydraulic system, the ideal flow rate values required to achieve maximum impact force from the jets and maximum hydraulic horsepower were determined. To maintain optimal drilling conditions, the drilling fluid flow rate should fall within this range between the two calculated values.

Table 3
Data with the lowest MSE in Dariyan layer.

TVD	WOB	RPM	MW	Q	PV	YP	ROP	MSE
1290.2	10	88	9.2	803	12	17	53.14	4878.9
1292.03	10	88	9.2	803	12	17	51.5	5032.7
1291.12	10	88	9.2	803	12	17	50.19	5162.9
1289.29	10	89	9.2	805	12	17	50.24	5187.5
1292.94	11	88	9.2	803	12	17	35.76	7949.7
1344.21	9	104	9.2	953	12	17	31.82	8623.2
1299.3	16	125	9.2	778	12	17	59.38	9902.8
1346.04	7	134	9.2	953	12	17	26.57	10329.7
1321.17	10	112	9.2	903	12	17	30.83	10642.1
1297.49	19	125	9.2	783	12	17	63.64	10977.9
1342.38	8	104	9.2	776	12	17	21.3	11419
1300.2	18	125	9.2	843	12	17	56.1	11786.9
Average of the best drilling parameters (Optimum parameters)								
1308.86	11.5	105.8	9.2	843	12	17	44.23	8491.11
Average of the all parameters in this formation (Applied parameters)								
1318.7	20.79	123.8	9.2	872.3	12	17	42.48	19476.1
Average of the worst drilling parameters (high MSE)								
1327.04	26.08	137.3	9.2	897	12	17	32.12	34070.2

$$Motor\ differential\ pressure = \frac{Torque}{k} = \frac{\left(\frac{\mu D_{Bit} WOB}{36}\right)}{k} = \frac{0.35 * 16 * 11500}{36 * 24.82}$$
$$= 72.1\ psi$$
(29)

Fig. 7 illustrates the variations in jet impact force and hydraulic horsepower with different flow rates while considering the presence of the mud motor. The hydraulic horsepower peaks at a flow rate of 795 gpm, while the maximum jet force is generated at 986 gpm. Flow rates ranging from 795 to 986 gpm represent the most favorable operational range. Consequently, the obtained average flow rate of 838.7 is optimal since it is in this range.

Subsequently, by utilizing the optimal flow rate, the optimal values for motor rotation speed and surface RPM were determined in the following manner.

$$RPM_{motor} = \frac{Q - Q_{Slip}}{q_0} = \frac{843}{9.125} = 92.38\ rev/min$$
(30)

$$RPM_{surface} = RPM_{Bit} - RPM_{motor} = 105.8 - 92.38 = 13.42\ rev/min$$
(31)

in some cases, according to field experience, the driller believes that the $RPM_{surface}$ should be at least 40 rpm; otherwise, the well cleaning will not
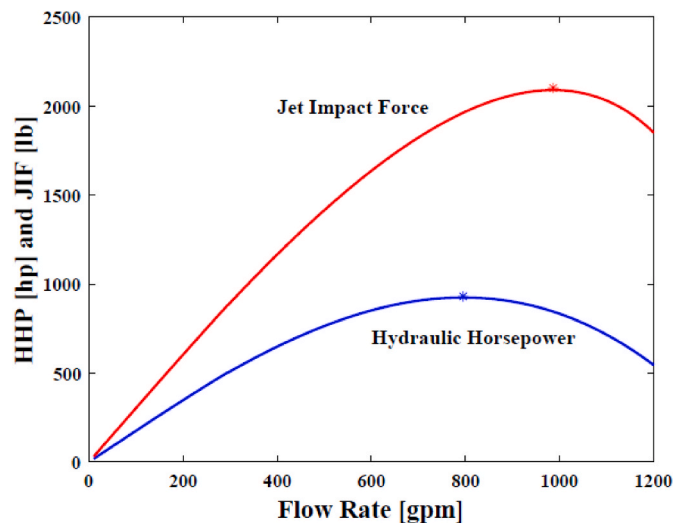

Fig. 7. The impact of flow rate on bit jet impact force and hydraulic horsepower.

be done correctly, or the torque of the drill pipe will increase. In this case, it is better not to calculate the $RPM_{surface}$ from Eq. (31) and set it equal to the value suggested by the driller because torque calculations and hole-cleaning are not included in this modeling. In this study, the well drilled in the Dariyan formation is a nearly vertical well. There is no problem regarding torque and hole cleaning, and the value obtained from Eq. (31) is acceptable. This problem is more challenging in deviated and horizontal wells.

5.2. Mathematical modelling approach

This section presents the objective functions for the mathematical modeling of the Dariyan formation, considering the mud motor's inclusion. The hydraulic power function described in Eq. (32) was utilized to optimize the flow rate of the hydraulic system. It is important to note that this study considers both hydraulic horsepower and jet impact force. This is because the jet impact force is a factor in the ROP, and the optimal flow rate is consistently achieved within the optimal range.

$$HP = \left(3200 - \left(\left(4.2 * 10^{-5} * MW^{0.8}.Q^{1.8}.PV^{0.2}\right) + P_{BHA} + \frac{\left(\frac{0.35*16*10^3*WOB}{36}\right)}{24.82}\right)\right) * Q$$
(32)

The data set shows that some variables have both a high ROP and MSE. The goal is to find variables with high ROP and low MSE. The MSE is one of the objective functions for this reason. Eq. (33) shows the MSE model that includes the mud motor.

$$MSE = \left(\frac{10^3 * WOB}{201}\right) + \left(\frac{120\pi}{201 * ROP}\right)\left(RPM_{Surface} + \left(\frac{Q}{9.125}\right)\right)\left(\frac{0.35 * 16 * 10^3 * WOB}{36}\right)$$
(33)

The ROP model for the Dariyan formation is shown in Eq. (34) to Eq. (36). The CCS of the rock is one of the parameters of this model. This study used a fixed number of 4000 psi for CCS. If the geo-mechanical variables of the rock are known more precisely, the model will be more accurate.

$$ROP = 622.54 * 0.877$$

$$* \left[\left(\frac{1.08978 * 10^{-6} 4000^2 16^3}{RPM_{Bit}.WOB^2} + \frac{477.74}{RPM_{Bit} * 16} \right) + \frac{36.324 * 16 * MW * PV}{8.33 * F_{jm}} \right]^{-1} \tag{34}$$

$$F_{jm} = \left(1 - \left(\frac{0.15 * 16^2}{3 * 0.625^2} \right)^{-0.122} \right) * \left(\frac{0.000516 * MW * Q * Q * 0.32}{0.92} \right) \tag{35}$$

$$RPM_{Bit} = RPM_{Surface} + \left(\frac{Q}{9.125} \right) \tag{36}$$

Fig. 8 shows how well this model estimates the ROP in the Dariyan formation.

5.2.1. Limitations

Performing optimization without taking into account the constraints can result in inaccuracies. It is essential to consider certain limitations. The upper and lower values of drilling parameters, which are obtained based on the analysis of the drilling data from previous drillings, are presented in Table 4.

Many problems during drilling occur due to inappropriate drilling parameters, such as vibration, buckling of pipes, stuck pipes, and bit failure [42]. Consequently, a careful analysis of daily drilling reports can reveal the parameters responsible for such problems. It is essential to establish parameter limits that exclude problematic values. In the case of Dariyan layer, there have been no reported problems, indicating that the parameters listed in Table 2 fall within a safe range. This study established parameter boundaries based on a combination of drilling data analysis, modeling outcomes and field experiences. For instance, during the drilling of this formation, flow rates were observed to fall within the range of 760–963 gpm, as indicated in Table 2. Additionally, modeling results presented in Fig. 7 showed that the optimal flow rates resided within 795–986 gpm. Consequently, the flow rate range was set at 795 to 963 gpm. The permissible range for surface rotation speed values was defined as 0 to 40, as indicated in Table 2. The drilling of the Dariyan layer in this particular well is susceptible to axial vibration, commonly called bit bouncing. According to drillers experiences, this phenomenon occurs due to using a tri-cone bit for drilling a limestone formation in a shallow near vertical borehole with a large diameter. Empirical evidence from drilling operations indicates that axial vibration phenomena reveal themselves under conditions characterized by high rotational speeds and low WOB values. Taking into account the data provided in Tables 2 and it is observed that the minimum WOB recorded in this particular borehole is 7000 lb. However, a minimum WOB of 10000 lb was considered appropriate to exercise an additional level of caution. It is essential to acknowledge that throughout the drilling process of the mentioned hole, as indicated in Table 2, the applied WOB within the range of 7000–31000 and the rotational speed within the range of

Table 4
The upper and lower boundaries of drilling parameters are based on drilling records.

Parameter	Lower limit	Upper limit
WOB (*klb*)	10	40
Bit RPM (rpm)	88	145
Surface RPM (rpm)	0	40
Flow rate (GPM)	795	963

88–145 rpm did not result in any problems. Consequently, a minimum WOB of 10000 was implemented as a precautionary measure. Ensuring that the maximum WOB remains below the motor's maximum differential pressure is essential. In this study, the motor's maximum differential pressure is 300 psi, and the pressure drop must not exceed this limit. The calculated maximum allowable WOB, obtained from Eq. (37), is 47860 lb. For safety, a maximum WOB of 40000 lb was used in this study to avoid motor damage.

$$\Delta P_{Stall} > \frac{\left(\frac{\mu D_{Bit} WOB_{Max}}{36} \right)}{k} \rightarrow 300 > \frac{\left(\frac{0.35 * 16 * WOB_{Max}}{36} \right)}{24.82} \rightarrow WOB_{Max} < 47860 \, lb \tag{37}$$

5.2.2. BHA information

In this well, the BHA listed in Table 5 has been used. The table below gives their internal and external diameters, as well as their length. The Bingham plastic model was employed to determine pressure loss in various sections of the drilling string. The casing pipe, with a diameter of 18.625 inches, is situated at a depth of 1087 m, with an inner diameter measuring 17.755 inches. The drilling fluid has a density of 9.2 ppg, a plastic viscosity value of 12 *cp*, and a yield point of 17 $lb/100ft^2$.

Table 5
The characteristics of utilized BHA.

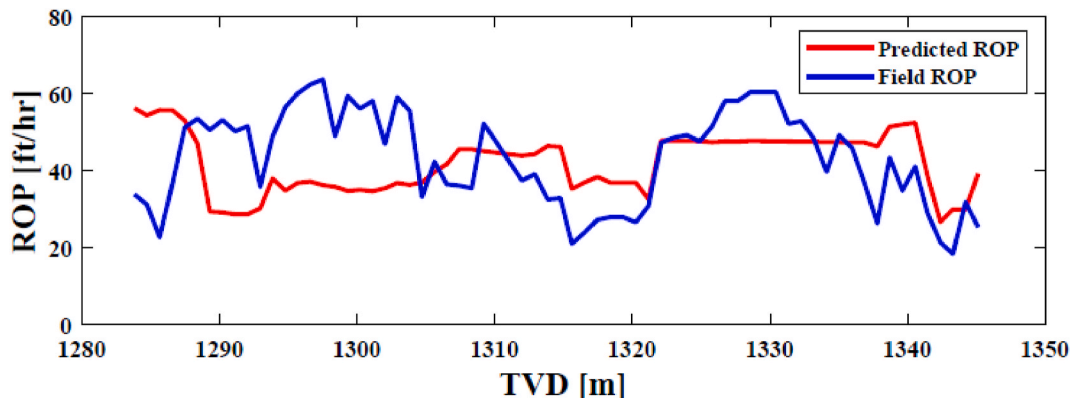| BHA	Length (m)	Inner diameter (in)	Outer diameter (in)
Bit	0.36	3	16
Motor	9.69	3	9.625
Float sub	0.84	2.8125	9.5
Stabilizer	2.72	2.75	9.5
UBHO	0.8	3	9.5
Non-magnetic drill collar	9.42	3.5	9.5
Drill collar	9.4	3	9.5
XO	0.91	3	9.5
8 ¼ Jts DC	74.55	3	8.25
Drilling Jar	9.57	2.8125	8.5
3 Jts 8″ DC	27.82	3	8.5
XO	0.91	3	8.5
9 JtsxHWDP	83.92	4	5.5
Drill pipe	1133	4.202	5

Fig. 8. Performance of the developed ROP model.

Moreover, the pump pressure is equal to 3200 psi.

The pressure drop in the equipment located within the well was determined by employing the Bingham plastic model and utilizing the correlations outlined in chapter 8 of Rabia's book (Appendix A) [39]. The graph in Fig. 9 illustrates the relationship between pressure drop and flow rate in downhole equipment.

5.2.3. Optimization process

To expedite the attainment of precise results, a thorough sensitivity analysis was conducted to identify the optimal parameters for the Genetic Algorithm (GA). This evaluation examined how the algorithm's efficiency was affected by the Crossover Probability, Mutation Rate, Population Size, and Pareto Fraction. The research findings revealed that increasing these parameters sometimes improves algorithmic performance.

5.2.4. Sensitivity analysis

5.2.4.1. Crossover probability.
As illustrated in Fig. 10, increasing the crossover probability has a detrimental effect on the algorithm's performance. Therefore, a value of 0.5 was selected for this study.

5.2.4.2. Mutation rate.
Within this study, a comprehensive sensitivity analysis was conducted to evaluate the impact of the mutation rate as an additional parameter. Fig. 11 portrays that an escalation in the mutation rate facilitates a broader solution for space exploration. Nevertheless, this expansion also entails an elongated processing time. As a means to strike a balance between search range and processing efficiency, the mutation rate was established at 0.2.

5.2.4.3. Population size.
The sensitivity analysis also assessed the influence of population size on the performance of the MOGA. Although a larger population has the potential to generate improved outcomes, it concurrently leads to an increase in computational time. Consequently, a population size of 150 was selected as a reasonable trade-off. Fig. 12 provides a graphical depiction of the MOGA's performance across various population sizes.

5.2.4.4. Pareto fraction.
A sensitivity analysis was performed to identify the ideal Pareto Fraction for the algorithm. The results indicated that choosing very low values, such as 0.1, produced inconsistent results with significant variations across different runs. Conversely, high values compromised accuracy and made it more challenging to find the optimal solution. By setting the Pareto Fraction to 0.3, we achieved a satisfactory
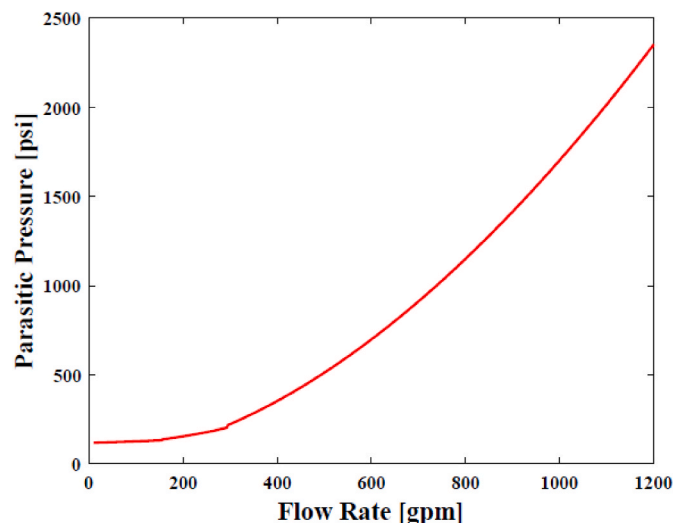

Fig. 9. The relationship between pressure drops and flow rate.

balance between accuracy and result repeatability. As a result, 0.3 was determined to be the optimal Pareto Fraction value for this study. Table 6 provides a list of the parameters that comprise the optimized algorithm.

The Multi-Objective Genetic Algorithm (MOGA) initiates with an initialization phase, creating a population of 150 solutions that adhere to specified constraints. In each loop iteration, the objective functions for every solution are computed, and fitness scores are assigned according to their performance. Within each generation, the Pareto optimal solutions secure the top rank, and a subset of these optimal solutions is selected to serve as parent solutions for the subsequent generation. A crossover operator modifies the selected parents to generate new solutions, aiming to discover fitter alternatives. These improved solutions take the place of low-ranked options with poor fitness scores. A mutation operator is applied to the parents, generating a new set of potential solutions for the later generation. The new solutions are accepted or rejected according to their fitness compared to the parents. This mutation step marks the end of each iteration. In this research, the procedure is iterated for 200 iterations. The goal is to minimize both torque and length objectives together. This leads to acquiring a cluster of solutions with similar values, known as the Pareto optimal solutions. These solutions can be graphically depicted as a Pareto frontier. The optimization process and Pareto frontiers are shown in Fig. 13.

The multi-objective optimization approach produces a collection of non-dominant Pareto solutions, requiring a decision-making process to identify the optimal solution from this set. This study employs a fuzzy decision-making technique to select the most favorable solution (tradeoff) among the non-dominant solutions located on the Pareto front. Eq. (38) is utilized to compute the fuzzy membership value of the objective function for the jth criterion [9,67–70].

$$\chi_j = \begin{cases} 1 & for\ OF_j < OF_j^{Min} \\ \left(\dfrac{OF_j^{Max} - OF_j}{OF_j^{Max} - OF_j^{Min}}\right) & OF_j^{Min} < OF_j < OF_j^{Max} \\ 0 & for\ OF_j > OF_j^{Max} \end{cases} \quad (38)$$

here, OF^{Min} and OF^{Max} denote the minimum and maximum fitness values of the objective functions, respectively. The mathematical expression in Eq. (39) represents the function χ^k, which calculates the degree of membership for each non-dominant solution [9,67,70].

$$\chi^k = \frac{\sum\limits_{i=1}^{N_{obj}} \chi_j^k}{\sum\limits_{k=1}^{ND} \sum\limits_{j=1}^{N_{obj}} \chi_j^k} \quad (39)$$

The expression in Equation (26) defines the normalized membership function χ^k for each non-dominant solution. Here, ND represents the number of non-dominated solutions, and N_{obj} represents the number of objective functions, which in this case are MSE, HHP, and ROP. The optimal solution can be determined by selecting the normalized membership function with the highest value of χ^k during this process.

The solutions exhibiting the highest χ^k values are chosen as the top solutions. The optimal drilling parameters resulting from the multi-objective optimization with the genetic algorithm and the fuzzy decision-making method for different runs are presented in Table 7. Due to its stochastic nature, the genetic algorithm exhibits variability in the obtained solutions across multiple runs. To achieve this objective, the findings were displayed for multiple successive runs. The results indicate that the acquired optimal values are close to each other.

Table 8 showcases the optimal solutions selected for the multi-objective optimization of drilling parameters for different runs. As can be seen, the algorithm converges to nearly close values of objective functions, but results are different in each run. The genetic algorithm has
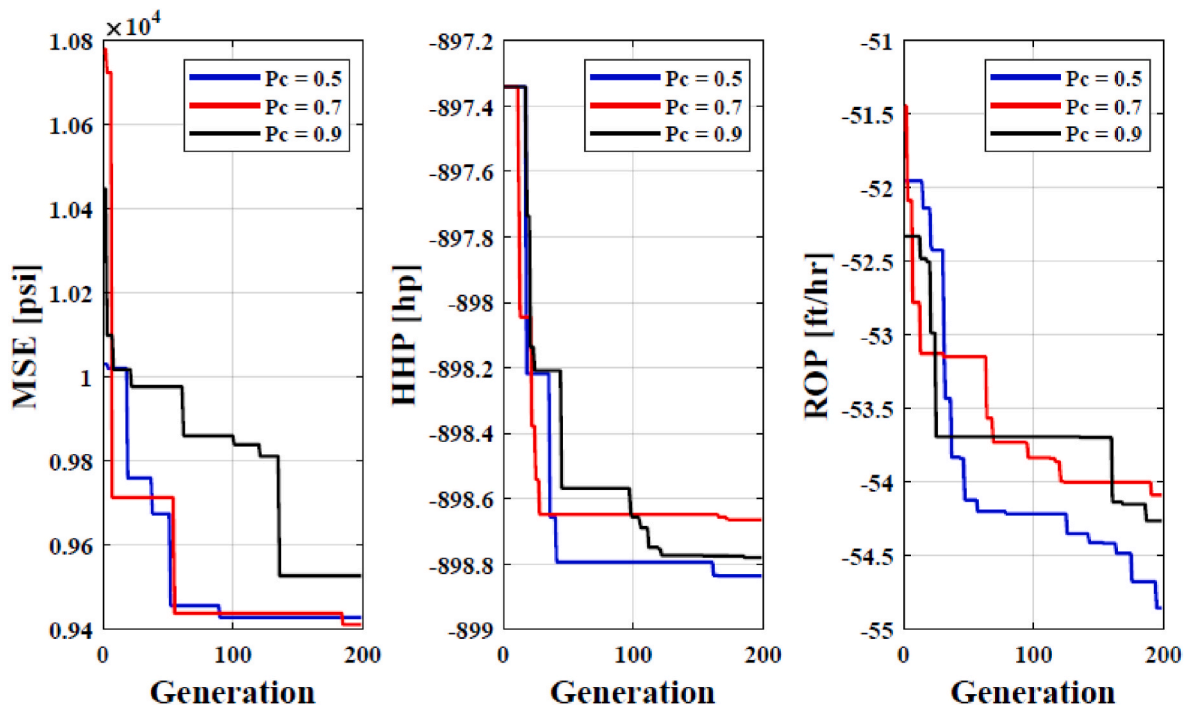
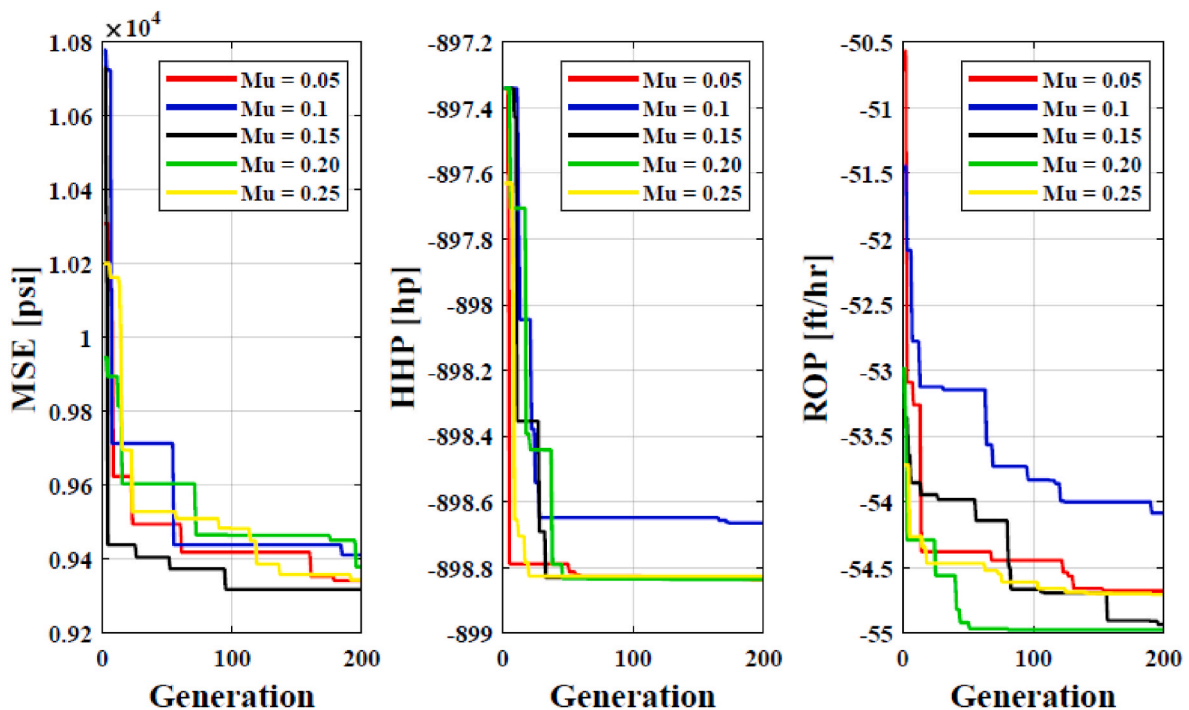**Fig. 10.** Effect of crossover probability on MOGA.

Fig. 11. Performance of MOGA in different mutation rates.

excellent and fast performance in finding the optimal solution, and each run takes less than 1 min, so it is a suitable tool for drilling optimization and can be used during drilling. Due to the random nature of the genetic algorithm, the answers in each run are slightly different from other runs, but it does not cause errors because the results from different runs are very close to each other.

The results show that data mining and mathematical optimization can detect the optimal variables. Both methods show that the optimal values of drilling parameters are not their maximum values. In some

cases, increasing drilling parameters consumes more work and more energy, the drilling efficiency decreases, and bit wear increases. The drilling data highly influence the data mining method, and its results are the average of the best parameters applied during drilling so the results are a little different from the multi-objective optimization method. Comparing the results with the drilling parameters in the Dariyan layer, it is evident that the MSE has dropped significantly, from an average of 19476.1 psi (Table 3) to 12436.42 psi and lower values (Table 8). This reduction signifies enhanced drilling operation.
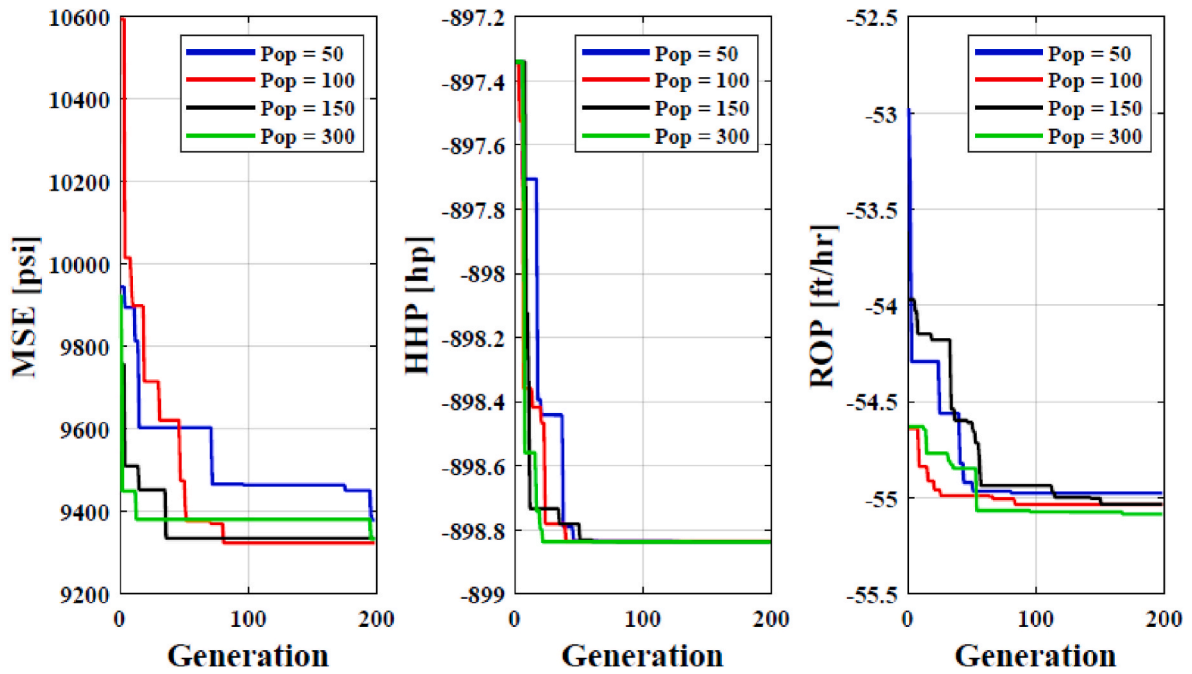
Fig. 12. Impact of population size on the performance of MOGA.

Table 6
Optimum parameters of MOGA.

No.	MOGA Parameter	Optimal Value
1	Crossover Probability	0.5
2	Mutation Rate	0.2
3	Population Number	150
4	Pareto Fraction	0.3
5	Generation	200

5.3. Validation of results

The case study in this research does not include pilot or field testing. The best method to check the accuracy of the results is to implement this method on a formation that is being drilled. However, by comparing the results of this method with the drilling data, their accuracy can be checked to some extent. For example, in this formation at a depth of 1298.39 m, the WOB of 19 *klb* and the rotation speed of 125 rpm have created a drilling speed 48.88 ft/h and MSE value of 14264.85 psi. Also, at a depth of 1321.17 m, the WOB of 10 *klb* and the rotation speed of
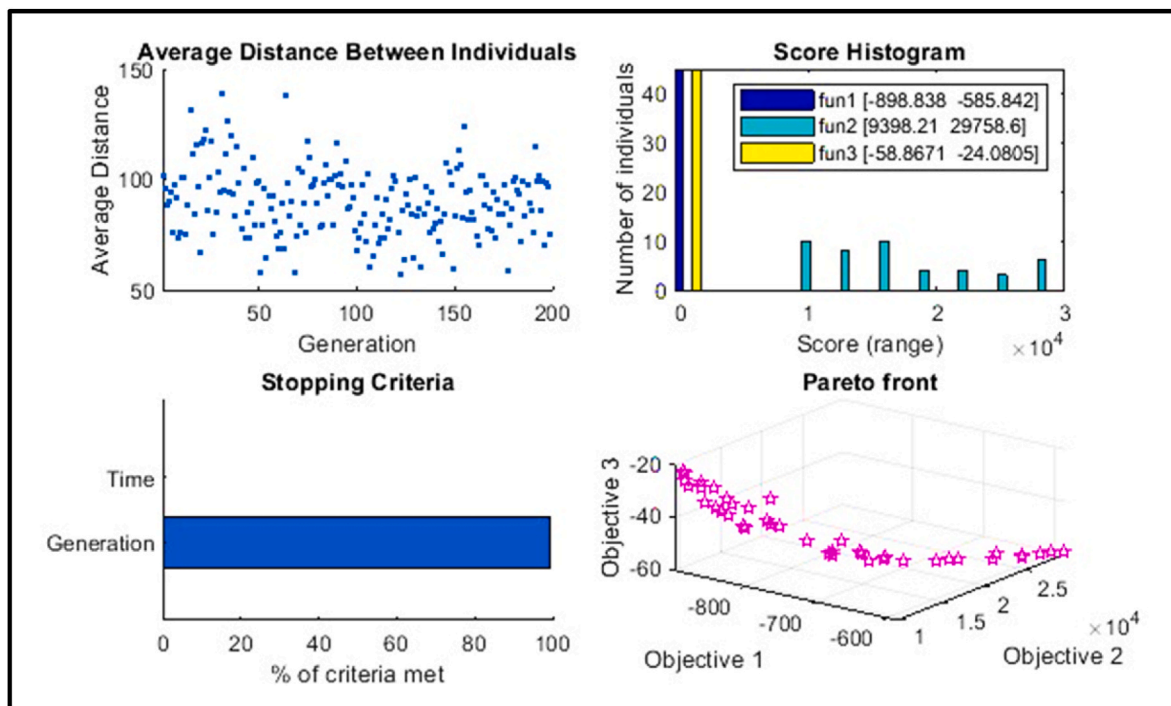

Fig. 13. The outcomes of the multi-objective optimization process.

13

Table 7
Optimal drilling parameters.

Parameter	WOB	RPM			Flow Rate
		Surface	Motor	Bit	
Unit	*klb*	*rev/min*	*rev/min*	*rev/min*	*gpm*
Run 1	15.17	10	103.53	113.53	944.7
Run 2	13.83	15.94	99.76	115.71	910.35
Run 3	16.61	9.11	103.13	112.24	941.1
Run 4	15.23	8.65	104	112.6	949
Run 5	14.48	14.17	100.91	115.08	920.87

Table 8
The chosen optimal solutions.

Objective Function	HHP	MSE	ROP	Drilling Efficiency
Unit	*hp*	*psi*	*ft/hr*	%
Run 1	810.1	11810.4	42.83	33.86
Run 2	841.28	12031.62	39.03	33.24
Run 3	802.82	12436.42	44.03	32.16
Run 4	806.5	11686.25	43.12	34.22
Run 5	830.82	12077.56	40.49	33.12

112 rpm have created a drilling speed 30.83 ft/h and MSE value of 10642.1 psi. In the obtained results, run three has made a WOB of 16.61 *klb* and a rotation speed of 112.24 rpm, a rate of 44.03 ft/h, and MSE value of 12436.42 psi. Moreover, drilling data show that at the depth of 1340.54 m, WOB of 28 *klb*, rotation speed of 143 rpm, and flow rate of 953 gpm produced a drilling speed of 41.01 ft/h and the MSE value of 14264.85 psi. Comparing this value with the optimal value shows that the results are reliable and efficient, and the multi-objective approach optimizes both the ROP and MSE in a specific formation and provides acceptable results that have optimal ROP and MSE, simultaneously.

5.4. Study constraints and future research prospects

One of the limitations of this research is the amount of data. The use of new methods to collect more data and advanced approaches to predict drilling problems increase the accuracy of optimization and enhance the drilling operation [71]. For example, Liu et al. used drilling microchips to measure the temperature and pressure during drilling [72]. As mentioned in the article, achieving a high level of precision in determining the geo-mechanical properties of the formation leads to more precise and reliable results, particularly in the domains of drilling speed modeling and drilling efficiency computations. It is also evident that as the accuracy of the drilling speed model increases, the optimization error decreases.

Furthermore, including calculations related to hole cleaning, torque, and vibrations significantly enhances the precision of the presented methodologies. In conventional drilling, these calculations may not be deemed essential. However, for drilling operations in deep wells, highly deviated wells, such as horizontal and extended reach drilling, it becomes imperative to use these calculations into the model. The reason is that these types of wells present challenges like high torque, inadequate hole cleaning, controlling well path during drilling, difficulty in transferring force to the bit [73–78]. Any of these issues can lead to drilling operation failures in such wells [9]. For example, the rotation speed of dill pipe directly impacts hole cleaning and cutting transport process [79] therefore, modeling this process and using it in the optimization process increase the accuracy and reliability of results.

6. Conclusion

This study introduces a data mining methodology and a multi-objective optimization method to improve drilling parameters and identify the optimal variables in a specific formation that is drilled using a positive displacement motor. The considered factors for optimization are ROP, MSE, and drilling hydraulics.

- In the context of traditional drilling, it is observed that the drilling parameters are independent. However, when utilizing a mud motor, the controllable parameters of the drilling process exhibit interdependence. For instance, altering the flow rate leads to a change in the RPM of the bit. This study appropriately models the impact of the mud motor on the ROP, MSE, and drilling hydraulics.
- Results showed that the data mining method had an excellent performance in determining data distribution and optimal and non-optimal parameters by using ROP, MSE, optimal flow rate window, and drilling efficiency, and it can be easily used in any drilling data set.
- According to the results, the mathematical optimization method outperforms the data mining approach. This is due to the substantial impact of drilling data on the data mining approach, which tends to generate optimal results solely within the range of drilling data but cannot extend beyond the range of available data. In contrast, the mathematical model evaluates all data points and calculates the most suitable parameters.
- The results of the data mining approach and the mathematical optimization method are always in the same range because the same data and models are used in both. The only difference between these two methods is that the data mining method examines only the available data, while the optimization method builds a model of the data and then examines all the points. In this research, the data mining results were 11.5 *klb* WOB, 105.8 rev/min rotation speed, and 843 gpm flow rate, resulting in 44.23 ft/h ROP. The best multi-objective optimization results were 14.48 *klb* WOB, 115 rev/min rotation speed, and 920.8 gpm flow rate, yielding 40.49 ft/h ROP. Optimal results show a significant MSE reduction of over 35 %.
- It is recommended that researchers increase the accuracy and reliability of this method and reduce the amount of error by considering the geo-mechanical properties of the formation in the model, torque and drag of the drill string, drilling vibrations, hole cleaning, and more accurate ROP estimation models.

Authors' contributions

H.Y.: Conceptualization, Methodology, Investigation, Software, Data curation, Visualization, Writing-Original Draft, M.F.: Conceptualization, Validation, Analysis, Supervision, B.S.A.: Conceptualization, Validation, Supervision, R.Kh.: Conceptualization, Validation, Supervision, J.Q.: Writing-Review & Editing, Validation, Funding, M.S.: Conceptualization, Advising, Validation, M.R.: Writing-Review & Editing, Validation.

Declaration of competing interest

The authors declare that they have no known competing financial interests or personal relationships that could have appeared to influence the work reported in this paper.

Appendix A

A.1 Inside pipes

In the initial phase, the average velocity and the critical velocity of the drilling mud flowing within the pipe are calculated by employing equations A1 and A2 correspondingly [39,41].

$$V^{'} = \frac{24.5 * Q}{D^2} \tag{A1}$$

$$V_C = \frac{97 * PV + 97\sqrt{PV^2 + 8.2\rho D^2 YP}}{\rho D} \tag{A2}$$

If $V^{'} > V_C$, then the flow is turbulent.

$$P = \frac{8.91 * 10^{-5}\rho^{0.8}Q^{1.8}PV^{0.2}L}{D^{4.8}} \tag{A3}$$

If $V^{'} < V_C$, then the flow is laminar.

$$P = \left(\frac{L.PV.V^{'}}{60000 * D^2}\right) + \left(\frac{L.YP}{225.D}\right) \tag{A4}$$

A.2 Inside annulus

Equations A5 and A6 are utilized to calculate the average velocity and the critical velocity of the drilling mud within the annular region [39,41].

$$V^{'} = \frac{24.5 * Q}{D_h^2 - OD^2} \tag{A5}$$

$$V_C = \frac{97 * PV + 97\sqrt{PV^2 + 6.2\rho D_e^2 YP}}{\rho D_e} \quad D_e = D_h - OD \tag{A6}$$

If $V^{'} > V_C$, then the flow is turbulent.

$$P = \frac{8.91 * 10^{-5}\rho^{0.8}Q^{1.8}PV^{0.2}L}{(D_h - OD)^3(D_h + OD)^{1.8}} \tag{A7}$$

If $V^{'} < V_C$, then the flow is laminar.

$$P = \left(\frac{L.PV.V^{'}}{60000 * D_e^2}\right) + \left(\frac{L.YP}{225 * D_e}\right) \tag{A8}$$

A.3 Pressure loss in surface equipment

The pressure drops in the surface equipment, including stand pipe, swivel, and Kelly can be calculated using equation (A9), and the constants of this equation are determined based on the type of surface equipment, as listed in Table A1 [39,41].

$$P_{surface} = E.MW^{0.8}.Q^{1.8}.PV^{0.2} \tag{A9}$$

Where ρ is density (ppg), Q is the flow rate (GPM), E is constant, PV is plastic viscosity (cp), and $P_{surface}$ is surface pressure drop (psi).

Table A1
The values of constant E for different types of surface equipment [39,41].

Type of surface equipment	E values	
	Metric units	Field units
1	0.0000088	0.000025
2	0.0000033	0.000096
3	0.0000018	0.000053
4	0.0000014	0.000042

Nomenclature

AI	Artificial Intelligence
BHA	Bottom hole assembly
CCS	Confined Compressive Strength, psi
CS	Cutter size, millimeters
D_{Bit}	Bit diameter, in
DDR	Daily drilling reports
DE	Drilling Efficiency, %
DGR	Daily geological reports
DMLR	Daily mud logging reports
F_{jm}	Modified jet impact force, klb
GA	Genetic Algorithm
GPM	Gallon per minute
HDI	Hydraulic drilling impact
HHP	Hydraulic horsepower, hp
JIF	Jet impact force, lb_f
MOGA	Multi-objective Genetic Algorithm
MSE	Mechanical specific energy, psi
MW	Mud weight, ppg
NPT	Non-productive time
NSGA-II	Nondominant sorting genetic algorithm-II
OF	Fitness value
PP	Pore pressure, ppg
PSO	Particle swarm optimization
PV	Plastic viscosity, cp
Q	Flow rate, gpm
RF	Random forest
RMSE	Root mean square error
ROP	Rate of penetration, ft/hr
RPM	Revolution per minute, rpm
T	Motor output torque, $lb.ft$
TFA	Total flow area, in^2
TOB	Torque on bit
TVD	True vertical depth, m
v	Speed of fluid exiting the drill nozzle, ft/sec
W_f	Bit wear function
WOB	Weight on bit, Klb
χ^k	Normalized membership function
YP	Yield point, $lb/100ft^2$
ΔP	Differential pressure of the motor, psi
μ	Sliding Friction coefficient, dimensionless

References

[1] J.-g. Li, K. Zhan, Intelligent mining technology for an underground metal mine based on unmanned equipment, Engineering 4 (3) (2018) 381–391.

[2] V. Zarei, et al., Implementation of Amorphous Mesoporous Silica Nanoparticles to formulate a novel water-based drilling fluid, Arab. J. Chem. 16 (8) (2023), 104818.

[3] K. Gao, et al., Modeling and experimental research on temperature field of full-sized PDC bits in rock drilling and coring, Energy Rep. 8 (2022) 8928–8938.

[4] L. Yongwang, et al., Experiment on the influence of downhole drill string absorption & hydraulic supercharging device on bottom hole WOB fluctuation, Energy Rep. 9 (2023) 2372–2378.

[5] H. Yang, et al., Wellbore multiphase flow behaviors during gas invasion in deepwater downhole dual-gradient drilling based on oil-based drilling fluid, Energy Rep. 8 (2022) 2843–2858.

[6] G. Li, et al., Intelligent drilling and completion: a review, Engineering 18 (2022) 33–48.

[7] M.A. Mirza, M. Ghoroori, Z. Chen, Intelligent petroleum engineering, Engineering 18 (2022) 27–32.

[8] X. Guo, et al., Theoretical progress and key technologies of onshore ultra-deep oil/ gas exploration, Engineering 5 (3) (2019) 458–470.

[9] H. Yavari, et al., Selection of optimal well trajectory using multi-objective genetic algorithm and TOPSIS method, Arabian J. Sci. Eng. (2023), https://doi.org/ 10.1007/s13369-023-08149-1.

[10] R. Khosravanian, B.S. Aadnoy, Methods for Petroleum Well Optimization: Automation and Data Solutions, Gulf Professional Publishing, 2021.

[11] W. Li, et al., Laboratory investigations on the effects of surfactants on rate of penetration in rotary diamond drilling, J. Petrol. Sci. Eng. 134 (2015) 114–122.

[12] M. Bajolvand, et al., Optimization of controllable drilling parameters using a novel geomechanics-based workflow, J. Petrol. Sci. Eng. 218 (2022), 111004.

[13] D. Sui, R. Nybø, V. Azizi, Real-time optimization of rate of penetration during drilling operation, in: 2013 10th IEEE International Conference on Control and Automation (ICCA), IEEE, 2013.

[14] A.M. Alali, et al., Hybrid data driven drilling and rate of penetration optimization, J. Petrol. Sci. Eng. 200 (2021), 108075.

[15] A. Shokry, S. Elkatatny, A. Abdulraheem, Real-time rate of penetration prediction for motorized bottom hole assembly using machine learning methods, Sci. Rep. 13 (1) (2023), 14496.

[16] M. Riazi, et al., Modelling rate of penetration in drilling operations using RBF, MLP, LSSVM, and DT models, Sci. Rep. 12 (1) (2022), 11650.

[17] M.R. Delavar, et al., Optimization of drilling parameters using combined multi-objective method and presenting a practical factor, Comput. Geosci. 175 (2023), 105359.

[18] E. Brenjkar, E.B. Delijani, Computational prediction of the drilling rate of penetration (ROP): a comparison of various machine learning approaches and traditional models, J. Petrol. Sci. Eng. 210 (2022), 110033.

[19] M. Sabah, et al., A machine learning approach to predict drilling rate using petrophysical and mud logging data, Earth Science Informatics 12 (2019) 319–339.

[20] F.J. Pacis, et al., Improving predictive models for rate of penetration in real drilling operations through transfer learning, Journal of Computational Science 72 (2023), 102100.

[21] Z. Fang, et al., Application of non-destructive test results to estimate rock mechanical characteristics—a case study, Minerals 13 (4) (2023) 472.

[22] M. Najjarpour, H. Jalalifar, S. Norouzi-Apourvari, Half a century experience in rate of penetration management: application of machine learning methods and optimization algorithms-A review, J. Petrol. Sci. Eng. 208 (2022), 109575.

[23] L.F.F. Barbosa, et al., Machine learning methods applied to drilling rate of penetration prediction and optimization-A review, J. Petrol. Sci. Eng. 183 (2019), 106332.

[24] A.A. Mahmoud, H. Gamal, S. Elkatatny, Evaluation of the wellbore drillability while horizontally drilling sandstone formations using combined regression analysis and machine learning models, J. Pet. Explor. Prod. Technol. (2023) 1–13.

[25] M.E. Hossain, A.A. Al-Majed, Fundamentals of Sustainable Drilling Engineering, John Wiley & Sons, 2015.

[26] C. Gan, et al., Prediction of drilling rate of penetration (ROP) using hybrid support vector regression: a case study on the Shennongjia area, Central China, J. Petrol. Sci. Eng. 181 (2019), 106200.

[27] C. Hegde, Rate of penetration (ROP) optimization in drilling with vibration control, J. Nat. Gas Sci. Eng. 67 (2019) 71–81.

[28] C. Hegde, K. Gray, Evaluation of coupled machine learning models for drilling optimization, J. Nat. Gas Sci. Eng. 56 (2018) 397–407.

[29] M.F. Al Dushaishi, et al., Selecting optimum drilling parameters by incorporating vibration and drilling efficiency models, in: SPE/IADC Drilling Conference and Exhibition, SPE, 2016.

[30] M.K. Moraveji, M. Naderi, Drilling rate of penetration prediction and optimization using response surface methodology and bat algorithm, J. Nat. Gas Sci. Eng. 31 (2016) 829–841.

[31] X. Chen, et al., Real-time optimization of drilling parameters based on mechanical specific energy for rotating drilling with positive displacement motor in the hard formation, J. Nat. Gas Sci. Eng. 35 (2016) 686–694.

[32] C. Hegde, et al., Fully coupled end-to-end drilling optimization model using machine learning, J. Petrol. Sci. Eng. 186 (2020), 106681.

[33] X. Liao, et al., Effects of a proper feature selection on prediction and optimization of drilling rate using intelligent techniques, Eng. Comput. 36 (2020) 499–510.

[34] A.R. Moazzeni, E. Khamehchi, Rain optimization algorithm (ROA): a new metaheuristic method for drilling optimization solutions, J. Petrol. Sci. Eng. 195 (2020), 107512.

[35] X. Wang, et al., A model-based optimization and control method of slide drilling operations, J. Petrol. Sci. Eng. 198 (2021), 108203.

[36] A. Bani Mustafa, et al., Improving drilling performance through optimizing controllable drilling parameters, Journal of Petroleum Exploration and Production 11 (2021) 1223–1232.

[37] C. Zang, et al., Drilling parameters optimization for horizontal wells based on a multiobjective genetic algorithm to improve the rate of penetration and reduce drill string drag, Appl. Sci. 12 (22) (2022), 11704.

[38] H.R. Motahhari, et al., Method of optimizing motor and bit performance for maximum ROP, J. Can. Petrol. Technol. 48 (6) (2009) 44–49.

[39] H. Rabia, Well Engineering & Construction, Entrac Consulting Limited London, 2002.

[40] M. Nystad, B.S. Aadnøy, A. Pavlov, Real-time minimization of mechanical specific energy with multivariable extremum seeking, Energies 14 (2021), https://doi.org/ 10.3390/en14051298.

[41] T.B. Adam, et al., Applied Drilling Engineering, vol. 2, SPE Textbook Series, Dallas, TX, 1991.

[42] V. Ramba, et al., Optimization of drilling parameters using improved play-back methodology, J. Petrol. Sci. Eng. 206 (2021), 108991.

[43] R. Ashena, et al., Improving drilling hydraulics estimations-a case study, J. Pet. Explor. Prod. Technol. 11 (6) (2021) 2763–2776.

[44] H.U. Caicedo, W.M. Calhoun, R.T. Ewy, Unique ROP predictor using bit-specific coefficient of sliding friction and mechanical efficiency as a function of confined compressive strength impacts drilling performance, in: SPE/IADC Drilling Conference, OnePetro, 2005.

[45] R. Pessier, M. Fear, Quantifying common drilling problems with mechanical specific energy and a bit-specific coefficient of sliding friction, in: SPE Annual Technical Conference and Exhibition, OnePetro, 1992.

[46] B.S. Aadnoy, Modern Well Design, CRC press, 2010.

[47] A. Raaen, et al., FORMEL: a step forward in strength logging, in: SPE Annual Technical Conference and Exhibition, OnePetro, 1996.

[48] R. Teale, The concept of specific energy in rock drilling, in: International Journal of Rock Mechanics and Mining Sciences & Geomechanics Abstracts, Elsevier, 1965.

[49] J. Huang, et al., Numerical study of rock-breaking mechanism in hard rock with full PDC bit model in compound impact drilling, Energy Rep. 9 (2023) 3896–3909.

[50] M. Rashidi, A. Asadi, An artificial intelligence approach in estimation of formation pore pressure by critical drilling data, in: ARMA US Rock Mechanics/ Geomechanics Symposium, ARMA, 2018.

[51] T. Warren, Penetration-rate performance of roller-cone bits, SPE Drill. Eng. 2 (1) (1987) 9–18.

[52] M. Rastegar, et al., Optimization of multiple bit runs based on ROP models and cost equation: a new methodology applied for one of the Persian Gulf carbonate fields, in: IADC/SPE Asia Pacific Drilling Technology Conference and Exhibition, OnePetro, 2008.

[53] G. Hareland, L. Hoberock, Use of drilling parameters to predict in-situ stress bounds, in: SPE/IADC Drilling Conference, OnePetro, 1993.

[54] W. Winters, T. Warren, E. Onyia, Roller bit model with rock ductility and cone offset, in: SPE Annual Technical Conference and Exhibition, OnePetro, 1987.

[55] H. Yavari, et al., Application of mathematical and machine learning models to predict differential pressure of autonomous downhole inflow control devices, Advances in Geo-Energy Research 5 (4) (2021) 386–406.

[56] Z. Sakhaei, E. Nikooee, M. Riazi, A new formulation for non-equilibrium capillarity effect using multi-gene genetic programming (MGGP): accounting for fluid and porous media properties, Eng. Comput. 38 (2) (2022) 1697–1709.

[57] H. Yavari, et al., Application of an adaptive neuro-fuzzy inference system and mathematical rate of penetration models to predicting drilling rate, Iranian Journal of Oil and Gas Science and Technology 7 (3) (2018) 73–100.

[58] A. Rabiei, et al., Determination of dew point pressure in gas condensate reservoirs based on a hybrid neural genetic algorithm, Fluid Phase Equil. 387 (2015) 38–49.

[59] F. Utaminingrum, et al., Feature selection of gray-level Cooccurrence matrix using genetic algorithm with Extreme learning machine classification for early detection of Pole roads, Results in Engineering (2023), 101437.

[60] S. Ghadami, et al., Optimization of multilateral well trajectories using pattern search and genetic algorithms, Results in Engineering 16 (2022), 100722.

[61] A.H. Moghaddam, et al., Multi-factor optimization of bio-methanol production through gasification process via statistical methodology coupled with genetic algorithm, Results in Engineering (2023), 101477.

[62] A. Santhosh, et al., Optimization of cnc turning parameters using face centred ccd approach in rsm and ann-genetic algorithm for aisi 4340 alloy steel, Results in Engineering 11 (2021), https://doi.org/10.1016/j.rineng, 2021.

[63] K. De Jong, Learning with genetic algorithms: an overview, Mach. Learn. 3 (1988) 121–138.

[64] J.H. Holland, Genetic algorithms, Sci. Am. 267 (1) (1992) 66–73.

[65] M. Mitchell, An Introduction to Genetic Algorithms, MIT press, 1998.

[66] A. Zoeir, et al., To optimize gas flaring in Kirkuk refinery in various seasons via artificial intelligence techniques, Sci. Rep. 13 (1) (2023), 13406.

[67] B.K. Das, et al., Techno-economic and environmental assessment of a hybrid renewable energy system using multi-objective genetic algorithm: a case study for remote Island in Bangladesh, Energy Convers. Manag. 230 (2021), 113823.

[68] S. Mondal, A. Bhattacharya, S.H. nee Dey, Multi-objective economic emission load dispatch solution using gravitational search algorithm and considering wind power penetration, Int. J. Electr. Power Energy Syst. 44 (1) (2013) 282–292.

[69] P.P. Biswas, et al., Multiobjective economic-environmental power dispatch with stochastic wind-solar-small hydro power, Energy 150 (2018) 1039–1057.

[70] A. Brka, Y.M. Al-Abdeli, G. Kothapalli, The interplay between renewables penetration, costing and emissions in the sizing of stand-alone hydrogen systems, Int. J. Hydrogen Energy 40 (1) (2015) 125–135.

[71] M. Amish, E. Etta-Agbor, Genetic programming application in predicting fluid loss severity, Results in engineering 20 (2023) 101464.

[72] H. Liu, et al., Application of drilling microchips for measurement of circulating pressure and temperature in vertical wells, Results in Engineering (2023), 101220.

[73] K. El Sabeh, et al., Extended-reach drilling (ERD)—the main problems and current achievements, Appl. Sci. 13 (7) (2023) 4112.

[74] A.L. Agbaji, Development of an Algorithm to Analyze the Interrelationship Among Five Elements Involved in the Planning, Design and Drilling of Extended Reach and Complex Wells, 2009.

[75] B. Saldivar, et al., An overview on the modeling of oilwell drilling vibrations, IFAC Proc. Vol. 47 (3) (2014) 5169–5174.

[76] A.S. Yigit, A.P. Christoforou, Stick-slip and Bit-Bounce Interaction in Oil-Well Drillstrings, 2006.

[77] K.-D. Chen, et al., Efficient and high-fidelity steering ability prediction of a slender drilling assembly, Acta Mech. 230 (2019) 3963–3988.

[78] A.J. Folayan, A. Dosunmu, B. Oriji, Microbial activity evaluation and aerobic transformation of deep water offshore synthetic drilling fluids in soil: a case study of ternary mixture of synthetic ethyl esters of plants oil (Seep mixture) synthetic drilling fluid in agbami (Niger delta) deep water field, Results in Engineering 15 (2022), 100537.

[79] N. Noroozi, M. Najjarpour, H. Jalalifar, Simulation of cutting transport process during foam drilling by implementation of computational fluid dynamics approach, Results in Engineering 18 (2023), 101081.